AAPS PharmSciTech, Vol. 15, No. 6, December 2014 (© 2014)
DOI: 10.1208/s12249-014-0170-3

Research Article

Synthesis of a Semi-Interpenetrating Polymer Network as a Bioactive Curcumin Film

Naeema Mayet,[1] Pradeep Kumar,[1] Yahya E. Choonara,[1] Lomas K. Tomar,[1] Charu Tyagi,[1] Lisa C. du Toit,[1] and Viness Pillay[1,2]

Received 17 February 2014; accepted 9 June 2014; published online 2 July 2014

Abstract. This study focused on the synthesis and characterization of a natural polymeric system employing the interpenetrating polymer network (IPN) comprising curcumin as a bioactive. Biopolymers and actives such as chitosan, hypromellose, citric acid, genipin, and curcumin were used to develop an effective, biodegradable, and biocompatible film employed therapeutically as a wound healing platform. The semi-IPN films were investigated for their physicochemical, physicomechanical, and biological properties by quantification by FTIR, DSC, and Young's modulus. Following characterization, an optimum candidate formulation was produced whereby further *in vitro* and *ex vivo* studies were performed. Results revealed a burst release occurring at the first hour with 1.1 mg bioactive released when in contact with the dissolution medium and 2.23 mg due to bioactive permeation through the skin, thus suggesting that the lipophilic nature of skin greatly impacted the bioactive release rate. Furthermore, chemical and mechanical characterization and tensile strength analysis revealed that the degree of crosslinking and concentration of polymeric material used significantly influenced the properties of the film.

KEY WORDS: biomaterials; crosslinker; curcumin; films; semi-interpenetrating polymer network; wound healing.

INTRODUCTION

Wound healing is a complex process and can be described as a function of the human body to replace injured and dead tissue with living cells. When the integrity of the skin structure and function is compromised, an intricate and dynamic process occurs known as the wound healing cascade which allows numerous matrix and cellular components to act together ensuring resurrection of the normal skin tissue (1). The primary target of wound care and management is to ensure that both the desirable clinical and pharmaceutical features for optimal treatment are improvised. These features would include wound closure, proliferation, debridement, absorption (2), esthetically acceptable scar, anti-bacterial and anti-inflammatory properties (3), angiogenesis, easy removal, and a moist wound environment (4). Currently, there are numerous wound healing products available for the treatment of burns, lacerations, incisions, chronic, and decubitus ulcers (5,6). However, there is a growing need for novel initiatives in the treatment of burn wounds and excessive skin loss (7). Novel wound dressing applications can be produced by the modification and synthesis of biocompatible materials. Biomaterials play a pivotal role in the wound healing process as they are biodegradable, biocompatible, bioadherent, and bioabsorbable, thus augmenting the healing process. In addition, they contribute inductive, instructive, stimulating, and triggering effects to the skin cells and tissues. Numerous synthetic and natural polymers have been used for wound dressing applications as follows: natural polymers include alginate (8), gelatin (9), collagen (10), and chitosan (11,12) and the synthetic polymers such as poly(ethylene glycol) (13), silicone rubber (14), and poly(amino acid) (15) have also shown to be useful for wound healing applications.

Chitosan (CS) is a natural polymer and a derivative of chitin which has many positive facets in the wound healing process such as biodegradability and excellent biocompatibility properties that are native to the body constituents (11,16). In addition, it is nontoxic and plays an imperative role in the wound healing process due to its versatile biological activity which includes the induction of the healing process within the regenerative and inflammatory phase and its ability to promote tissue growth and differentiation within skin tissue (17). Throughout the tropical regions such as South East Asia, Africa, India, and china, the cultivation of *Curcuma longa* has been widely established. *C. longa* also known as turmeric belongs to the *Zingiberace* family and is a perennial herb known to humankind for over 6,000 years (18). Within the biological and medical field, of particular interest are the phytochemical constituents such as curcuminoids and curcumin for their wide spectrum of biological activities. "Tumeric" or curcumin is a yellow rhizome which is extensively used in the food industry as a coloring and flavoring

[1]Wits Advanced Drug Delivery Platform Research Unit, Department of Pharmacy and Pharmacology, School of Therapeutic Sciences, Faculty of Health Sciences, University of the Witwatersrand, 7 York Road, Parktown, Johannesburg, 2193, South Africa.
[2] To whom correspondence should be addressed. (e-mail: Viness.Pillay@wits.ac.za)

agent, condiment and spice (19). Furthermore, traditional medicine practitioners of the tropical regions utilized curcumin to treat inflammation, urinary tract infections, hypertension, and eczema (20), in addition to being used as an antioxidant and anticancer agent (21). Current extensive studies and understanding of the phytochemical constituents of curcumin has led to the discovery of biological activities associated to appropriate wound healing such as anti-inflammatory and antioxidant properties. Furthermore, studies conducted in various animal models have proven curcumin to be nontoxic at even high doses (18). Curcumin, moreover, has been shown to play an important role in wound repair by ensuring the induction of TGF-β1 within the wound thus significantly enhancing the healing process (11,22,23). Hypromellose, a natural polymer, is known for its advantageous hygroscopic properties thus ensuring lubrication and providing an essential moist wound environment during the wound healing process. Hypromellose also promotes angiogenesis at the wound site, is nontoxic, and highly viscous, thereby registering sustained release of biopolymers by acting as a viscous barrier and controlling the rate of hydration and diffusion (24). Many polymers including the natural polymers have major drawbacks such as poor mechanical properties and rapid degradation which limits their application in the skin and tissue engineering field. Interest in the use of genipin as a crosslinker is on the increase due to the many toxic effects of other chemical crosslinkers such as glutaraldehyde (25), glyoxal (26), epichlorohydrin (27), and formaldehyde (28). Genipin is extracted from the *Gardenia jasminoides* fruit and is an iridoid glucoside that has been used by the food industry and Chinese traditional medicine as a blue colorant. It can crosslink macromolecules such as polysaccharides and proteins and is a well-known crosslinker of chitosan, a natural polymer consisting of many amino groups. The degree of crosslinking by genipin is mainly dependent on the availability of free amino groups to which it can react under mild conditions and can clearly be noted by the blue color change that occurs upon crosslinking (29,30). In comparison to other potent crosslinkers as mentioned above, genipin can produce crosslinked materials with comparative degradative and mechanical properties (30). Within the field of biotechnology and biomaterials, Genipin is widely employed in studies related to tissue engineering, regeneration, and fixation. In addition, it has been used in the formation of interpenetrating polymer networks (IPN), nanocomposites, nanoparticles, as well as microspheres and macrogels (29). Of particular interest in this study is its use as a natural crosslinker to form a semi-interpenetrating polymer network (s-IPN) whereby it also provides further advantageous therapeutic benefits relating to wound healing such as anti-inflammatory properties (30).

The addition of a cross-linker such as genipin can greatly improve upon or overcome these drawbacks. Furthermore, genipin is nontoxic and biocompatible, thus it has been shown to be an effective crosslinking agent of both biomaterials such as chitosan, containing a large amount of amino groups and the natural cellular tissue (31–33).

In preparing a wound dressing, the combination of various complementary biopolymers that have the capability to additively accelerate the healing process as well as optimizing the beneficial effect of each individual entity is essential (13,34). To achieve this, an IPN structure which is described at the molecular level as two or more polymer components interlaced in order to form a network that cannot be broken unless the individual entities are chemically separated is considered a viable option (35–37). The formation of an IPN ensures that components remain interlaced and there is a resistance to phase separation (38). In this study, the formation of a semi-interpenetrating polymer network was implemented in order to form films with the use of all natural biopolymers, crosslinkers, and bioactives which are chitosan, hypromellose, citric acid, curcumin, and genipin. These reagents can be combined to form films that have a synergistic healing effect throughout the phases of wound healing. In addition, all polymers and reagents used are biodegradable, biocompatible, nontoxic, and adherent.

MATERIALS AND METHODS

Materials

Chitosan (CS) (medium Mw poly(D-glucosamine) deacetylated chitin), hypromellose-hydroxymethylcellulose 2910, citric acid (ACS reagent ≥99.5%, Mw=192.12 g/mol), genipin (≥98% HPLC grade) powder (Mw=226.23 g/mol), and curcumin as well all other reagents of analytical grade used were procured from Sigma-Aldrich Chemie GmbH (Steinheim, Germany).

Synthesis of a Semi-Interpenetrating Network Polymer Film

Semi-interpenetrating network (IPN) polymer blends were prepared using the sequential IPN method. Various concentrations of chitosan (CS) ranging from 1 to 3% were added to a 5% (5 g/100 mL) solution of citric acid. This was then allowed to stir using a magnetic stirrer until a homogenous solution was formed. Next, the crosslinker genipin was dissolved in deionized water to make an aqueous solution of varying concentrations between 0.1 and 0.4%. This was then added to the CS solution to allow crosslinking. Thereafter, various concentrations of hypromellose solution ranging between 0.4 and 1.6% added to a 1% curcumin solution were mixed with the above blend. Lastly, 1 mL of glycerol was added to 40 mL of the s-IPN formulation consisting of all polymers, including the bioactive curcumin and crosslinker genipin and allowed to stir overnight to form a homogenous semi-IPN blend. The optimum quantity of each blend (10 mL) was poured into a rectangular mold composed of Parafilm (710×260 mm) and cast in film form by solvent evaporation at room temperature with the use of a fume hood under the influence of continuous airflow. After drying, semi-IPN films were removed from the fume hood and placed in a petri dish until further use under Parafilm. A three-factor Box-Behnken experimental design as shown in Table I (acquired from preformulation studies) was generated to obtain optimal concentration combinations of biopolymers in order to perceive optimal parameters from the design to acquire a semi-IPN film with superlative therapeutic and formulation outcomes. Preformulation experiments led to the search of variables that enabled an upper and lower limit of all factors necessary as shown in Table II to be established in order to run an accurate design. Furthermore, characterization of the design formulations lead to the establishment of an optimized semi-IPN film of optimal concentrations that is adequate as a wound dressing and further *in vitro* and *ex vivo* studies were conducted.

Table I. Box-Behnken Design Template for Statistically Derived Semi-IPN Film Formulations

Formulation no.	Chitosan (% *w/w*)	Genipin (% *w/w*)	Hypromellose (% *w/w*)	Curcumin (% *w/w*)
1	1	0.25	0.4	1
2	3	0.1	1	1
3	2	0.1	1.6	1
4	1	0.25	1.6	1
5	2	0.25	1	1
6	2	0.4	0.4	1
7	3	0.25	0.4	1
8	2	0.25	1	1
9	3	0.4	1	1
10	1	0.4	1	1
11	1	0.1	1	1
12	2	0.4	1.6	1
13	2	0.1	0.4	1
14	2	0.25	1	1

Characterization of the Semi-IPN Films for Wound Healing

Chemical Structure Analysis by Fourier Transform Infrared Spectroscopy

ATR-FTIR analysis, which identifies absorption bands based on vibrational molecular transitions, was conducted to characterize complex interactions occurring within bioactive polymer exchanges. A PerkinElmer® Spectrum 100 Series Fourier transform infrared (FT-IR) spectrometer fitted with a universal ATR Polarization Accessory (PerkinElmer Ltd., Beaconsfield, UK) was employed and Spectra over the range 4,000–625 cm^{-1}, with a resolution of 4 cm^{-1} and 32 accumulations was recorded for all semi-IPN film samples.

Thermodynamic Property Analysis by Differential Scanning Calorimetry Studies

Differential scanning calorimetry (DSC) measurements were taken for semi-IPN film samples weighing 7–10 mg using an advanced DSC (TMDSC/ADSC) (Mettler Toledo DSC-1 STAR^e System, Schwerzenback, ZH, Switzerland) at a heating rate of 10°C/min from −10 to 350°C under a nitrogen atmosphere. Weighed samples were placed in a covered aluminum sample holder with a central pin hold. Calibration of the DSC modulus was done in respect to enthalpy and temperature. Thermoanalysis of the samples was carried out with regard to the glass transitions, melting points, chemical reactions, and phase change temperatures of the polymeric system.

Table II. Template Exhibiting Upper and Lower Limits Derived from Preformulation Experimentation

Biopolymer/crosslinker	Upper limit	Lower limit
Chitosan	3%	1%
Hypromellose	1.6%	0.4%
Genipin	0.5%	0.1%

Surface Morphological Analysis by Scanning Electron Microscopy Imaging

Surface topographical structure of the dry semi-IPN films was analyzed by Scanning Electron Microscopy (SEM; Phenom™, FEI Company and Hillsboro, OR, USA) for porosity, surface roughness, and particle size of films. Samples were cut from films and mounted into metal stubs whereby samples were gold coated with an in-house SPI-Module Sputter Coater (SPI Supplies, Division of Structure Probe Inc., West Chester, PA, USA) prior to analysis.

Determination of the Physicomechanical Properties by Textural Profile Analysis

Semi-IPN film samples were subjected to texture analysis using a highly sensitive texture analyzer (TA.XT*plus* Texture Analyzer, Stable Microsystems, Surrey, UK) fitted with a 50-kg load cell. The physicomechanical properties of the film was measured by fixating film samples between two brackets placed 3 cm apart and a tension force of 0.5 mm/s applied to the system to determine the force at breaking point. This approach was employed to generate force-distance profiles to determine the tensile strength and work of extensibility which can be computed from the peak tensile force required and using Eq. 1. The parameters marked for textural analysis are presented in Table III. Tensile strength was measured using the Young's modulus.

$$E = \frac{\text{Tensile stress}}{\text{Tensile strain}} = \frac{\delta}{\varepsilon} = \frac{FL_o}{A_o \Delta L} \quad (1)$$

Where E = Young's modulus (modulus of elasticity), F = force applied to the object, A_0 = original cross-sectional area (πr^2) through which the force is applied, ΔL = quantity by which the length of the object changes, and L_0 = original length of the object.

Durability Testing of the Films by Nano-Tensile Mapping

The tensile properties (at a nanosensitivity level) of the semi-IPN films were evaluated using a nano-Tensile Analyzer (NanoTensile™ 5000, Hysitron Inc., MN, USA). Samples were mounted within nanotensile brackets that were held rigidly together by a frame, thus aiding in sample alignment and positioning. An accurate measurement of the width, thickness, and length of all film samples were taken using a digital caliper prior to mounting of samples. To determine the Young's modulus, brackets were made to move apart at a constant rate of 5 μm s^{-1} until a breaking force was established.

Table III. Parameters Employed for Textural Analysis

Parameters Settings	Settings
Test mode	Tension
Pre-test speed	0.50 mm/s
Test speed	0.50 mm/s
Post test speed	5.0 mm/s
Trigger type	Auto
Trigger force	5 kg
Contact time	5 s

Determination of the Swelling Capacity and Equilibrium Water Content

Preweighed samples of the semi-IPN films were dispersed in 15 mL of phosphate buffer solution (PBS; pH 7.4) and allowed to equilibrate at room temperature (21°C) for 24 h. Samples were then removed periodically at 1-h intervals, excess buffer was removed, and samples were reweighed. The swelling capacity (%) and equilibrium water content was determined using Eqs. 2 and 3 (39).

$$\%\ \text{Swelling Capacity} = \frac{\text{Final Weight} - \text{Initial Weight}}{\text{Initial Weight}} \times 100 \quad (2)$$

$$\%\ \textit{Equillibrium Water Content} = \frac{Ws - Wd}{Wd} \times 100 \quad (3)$$

Where W_s = weight of film in the swollen state when dispersed in deionized water and W_d = weight of film in the dry state after been dispersed in deionized water (hourly).

Analysis of the Water Vapor Transmission Rate into the Semi-IPN Films

Water vapor transmission rate (WVTR) tests were performed. Film samples were placed on the top of glass Polytops having an area of 144 mm^2 and containing 10 mL of phosphate buffer solution of pH of 7.4. This setup was preweighed and then placed in an oven at 35°C for 24 h. Samples were then reweighed at regular intervals and a plot of weight loss due to vapor transmission *versus* time was deduced. The transmission rate was determined using Eq. 4.

$$WVTR = \frac{wi - wt}{A} \times 10^6\ \text{g/m}^2\text{day}^{-1} \quad (4)$$

Where WVTR is expressed in g^2 h, A = area of the polytop opening (mm^2), wi and wt = the weight of the polytop before and after been placed in the oven, respectively (40).

Measurement of the Rheological Properties of the Semi-IPN Polymer Blends

A Haake Modular Advanced Rheometer System (MARS) (ThermoFisher Scientific, Karlsruhe, Germany) was used to determine the rheological parameters of the polymer solution blends employed for formulating the semi-IPN films. Samples were placed on a sample stage whereby a C35/1° titanium rotor was immersed in the polymer solution at a temperature maintained at 24°C, shear rate at 100 s^{-1}, and a time period of 360 s (41). Stress–strain rheological parameters were then obtained for all samples quantified.

Bioevaluation of the Semi-IPN Films for Wound Dressing Application

In vitro Release of Bioactive

The release of bioactive curcumin from the semi-IPN films was performed in a modified Franz diffusion cell (FDC) apparatus study setup. Films were cut in a circular section and placed on the receptor compartment to allow diffusion, which had a surface area of approximately 1.8 cm^2. Each receptor compartment was filled with 12 mL of isotonic phosphate buffer solution and was further thermoregulated at 37°C by a water jacket throughout the study. Receptor compartments were constantly stirred using a magnetic stirrer. At time periods 0.5, 1, 2, 3, 4, 6, 8, 10, and 12 h, 0.1 mL of solution was withdrawn from the receptor compartment and replaced by an equal quantity of fresh PBS buffer immediately after each sampling. Samples were then evaluated using a nanophotometer (Implen, GmbH, Munich, Germany) at a wavelength of 425 nm.

Ex vivo Permeation Studies Through the Sprague Dawley Rat Skin Model

Permeation studies were undertaken using skin excised from Sprague-Dawley rats. Rats were euthanized using pentobarbitone intraperitoneally (i.p) and the skin was carefully removed. Rat skin was stored in isotonic buffer solution at −80°C until further use. Prior to experimental procedures, skin was removed and thawed by placing in water at 37°C. The dorsal region was shaved and further subcutaneous and adipose tissue was carefully incised (42). Skin sections were excised to fit receptor compartments having a surface area of approximately 1.8 cm^2. To ensure that the integrity of the skin sections was maintained throughout the study, electrical resistance was measured across the skin membrane before and after permeation studies. This was performed by passing a fixed current across the skin preparation using a Mettler Toledo Seven Multi GmbH, Analytical CH-8603 Schwerzenbach, Switzerland connected to an electrode that was adjusted to isotonic environments by placing the probe into isotonic PBS solution before insertion with skin sections. Thereafter, the resistance and conductance measurements were taken as shown in Table IV at a temperature of 37°C (43).

The prepared skin was then placed between the donor and receptor compartment of the FDC apparatus. Semi-IPN films having a surface area of approximately 1.8 cm^2 was then placed over the skin and covered by the upper compartment of the FDC. Experimental procedures were performed as outlined for the *in vitro* bioactive release studies. The concentration of permeated curcumin was then determined using a nanophotometer (Implen, GmbH, Munich) whereby the extent of bioactive permeation across the membrane was evaluated by computing the drug flux. The flux (mg cm^{-2} h^{-1}) of curcumin across the skin tissue was calculated per unit area by linear regression analysis of permeation data using Eq. 5.

$$Js = \frac{Qr}{A \times t} \quad (5)$$

Where Js = the flux, Qr (mg) = the quantity of drug within the receptor compartment that has diffused through the skin, A (cm^{-2}) = the effective cross-sectional area that is available for permeation, and t (h) = the time of drug exposure to the skin tissue.

RESULTS AND DISCUSSION

FT-IR Chemical Structure Stability Analysis

Physical and chemical interactions involved in IPN formation of various polymer blend concentration were

Table IV. Resistance and Conductivity of Skin Preparations to Determine Skin Integrity Before and After *Ex Vivo* Permeation Studies

Skin preparation	Resistance (Ω/cm)	Conductivity (μs/cm)
Before	0.37×10^3	18
After	0.86×10^3	68

evaluated using FT-IR, which determined the degree of modification within the native polymers. The crosslinking within the films were characterized by the change in color from yellow (due to bioactive incorporation) to a dark deep green when crosslinked with genipin. Furthermore, the disappearance of a peak, at 1,223.62 cm^{-1}, representative of C-O stretching within the aromatic ring, upon crosslinking indicated the formation of a crosslinking bridge at the aromatic site of genipin with chitosan (CS) supporting the formation of a crosslinked network. Furthermore, O-H stretching indicated by the large broad band at 3,260.11 cm^{-1} was observed shifting to 3,278.79 cm^{-1} and absorbance from 0.34–0.35 A when crosslinked suggesting an increase in conjugation and intensity, impacting improved stability and physicomechanical properties to the film. It can further be deduced that a change in polymer concentrations resulted in a slight change within the spectra. A broad strong band representing hydrogen bonding for O-H stretching within the range of 3,200 and 4,000 cm^{-1} was observed with all semi-IPN films. A shift within the spectrum varied with the degree of crosslinking. Film 9 displayed a wavelength at 3,923.54 cm^{-1}, whereas a wavelength of 3,289.37 and 3,268.02 cm^{-1} was present in films 1 and 2, respectively (annotated in Fig. 1), characteristic to the bioactive curcumin indicating that an increase in crosslinker concentration resulted in a shift to a greater wavelength thus promoting conjugation and bond formation. In addition, the absence of a peak at the wavelength of 1,281.98 cm^{-1}, representative of the presence of an additional amino group in film 1, indicated no presence of free amino groups as seen with films 2, 5, 9, and 10. This was due to low CS concentration and more crosslinker, thus the formation of steric hindrance ensuring no presence of free amino groups. Film 5 showed the presence of a band at 1,980.69 cm^{-1} (demarcated in Fig. 1), which was not characteristic of any polymer entity but representative of the formation of C=C conjugation asymmetrical stretch and occurs when an intermediate amount of polymer entities are used thus the formation of intermolecular bonds.

Semi-IPN formation resulted in significant differences in infrared absorption frequencies of the final product in relation to the original compounds. Network formation resulted in a change in the vibrational energy and frequency thus the presence of skeletal vibrations at wavelengths of 2,937.54 and 2,881.46 cm^{-1} which were characteristic of C-H stretching and at 1,712.30 cm^{-1} characteristic of C=O stretching was noted. C-H bending within the aromatic ring was seen at wavelengths 921.85, 808.96, and 621.69 cm^{-1} related to the incorporation of a C-N group in place of the C-O group within the ring due to crosslinking. C-N stretching is also present at the wavelengths of 1,318.16 and 1,280.60 cm^{-1}. These peaks occur at higher vibrational frequencies and are associated with the degree of polymer network formation as well as crosslinking resulting in a change within the structural environment. As the concentration of crosslinker increased so

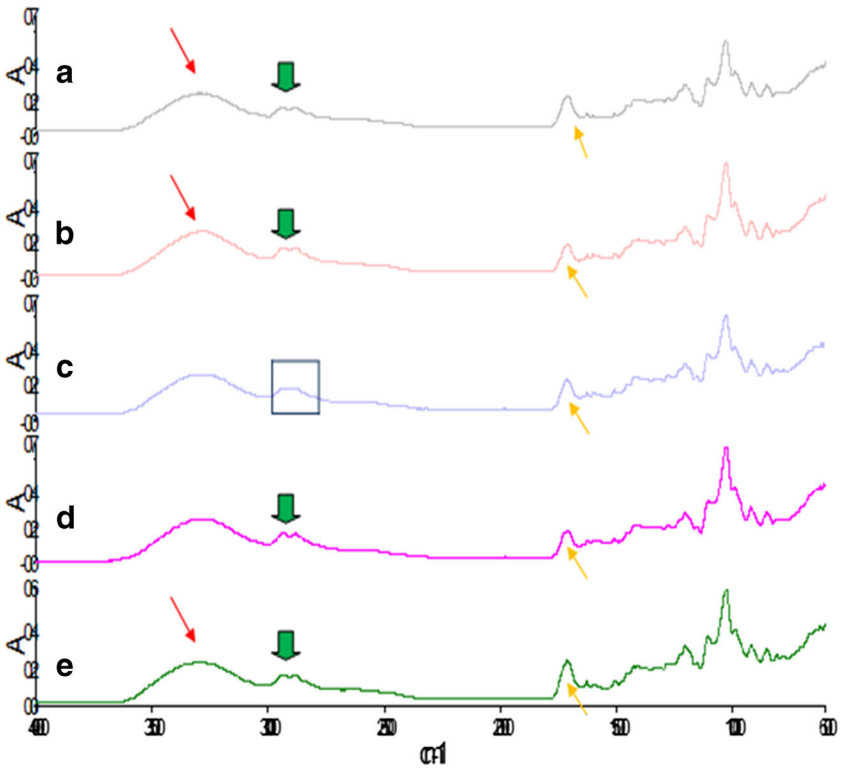

Fig. 1. Fourier transform infrared spectroscopy of semi-IPN films: **a** film 1, **b** film 2, **c** film 5, **d** film 9, and **e** film 10

did the intensity of the band formation, resulting in stretching and conjugation within the structure and bending between C-H bonds in the aromatic ring. Formulations displaying greater band intensities corresponded to a higher degree of crosslinking. Hence, it can be deduced that the degree of semi-IPN film formation was affected largely by the polymers and crosslinker concentration.

Assessment of the Thermodynamic Behavior of the Semi-IPN Films

The DSC thermograms of the various films showed a glass transition temperature (Tg) ranging between 28 and 30°C as shown in Fig. 2. This was related to a change in heat capacity when a transition occurred due to network formation and crosslinker concentration. Film 1 presented with the greatest Tg value due to the presence of amino groups capable of crosslinking at the temperature of curing. Film 1 also exhibits semicrystalline behavior, therefore affecting the mobility of the amorphous region influencing a higher Tg value. In addition, the degree of crosslinking affected the amorphousity of the structure; the highest Tg was thus observed in film 1 that had amino groups within the structure capable of crosslinking at the temperature of curing. A decrease in the degree of crosslinking due to crosslinker concentrations lower than the optimum was seen in film 2 resulted in a lower Tg value, thus was likely to display a quicker onset of degradation. Film 10 which had the highest recorded crystalline temperature of 213.96°C (displaying a more ordered molecular arrangement) resulted in decreased molecular motion, whereas film 9 (demarcated in Fig. 2) has a lower degree of crystallinity at 128.19°C. These observations are attributed to lower polymer concentration in Film 10 while higher polymeric concentrations were present in film 9, thereby varying the degree of crosslinking. This suggested that film 10 had a greater degree of regular molecular arrangements due to the formation of inter- and intramolecular bonds when lower polymeric concentrations are used, therefore a well-defined structure was obtained. Furthermore, film 10 also displayed the lowest degree of decomposition at a high-temperature range of 213.96°C which was attributed to its crystalline state. Film 9 on the other hand displayed a lower degree of crystallinity that was related to the random orientation of molecules displaying amorphous behavior due to free non-crosslinked groups within the structure with a poor polymer backbone. In addition, the amorphous form of film 9 was linked to the lack of crosslinking (curing) as displayed by the exothermic peak which preceded the endothermic melting transition phase present in all films (see film 6) showing semicrystalline behavior. Furthermore, the data obtained from the differential scanning calorimetry profiles reveal that all formulations degrade between a temperature rate of 230 and 300°C; this is largely due to the known fact that natural polymers are highly biodegradable due to properties such as their hydrophilic nature, they are easily swellable and water wettable as well as greatly sensitive to temperature changes, thus they tend to degrade

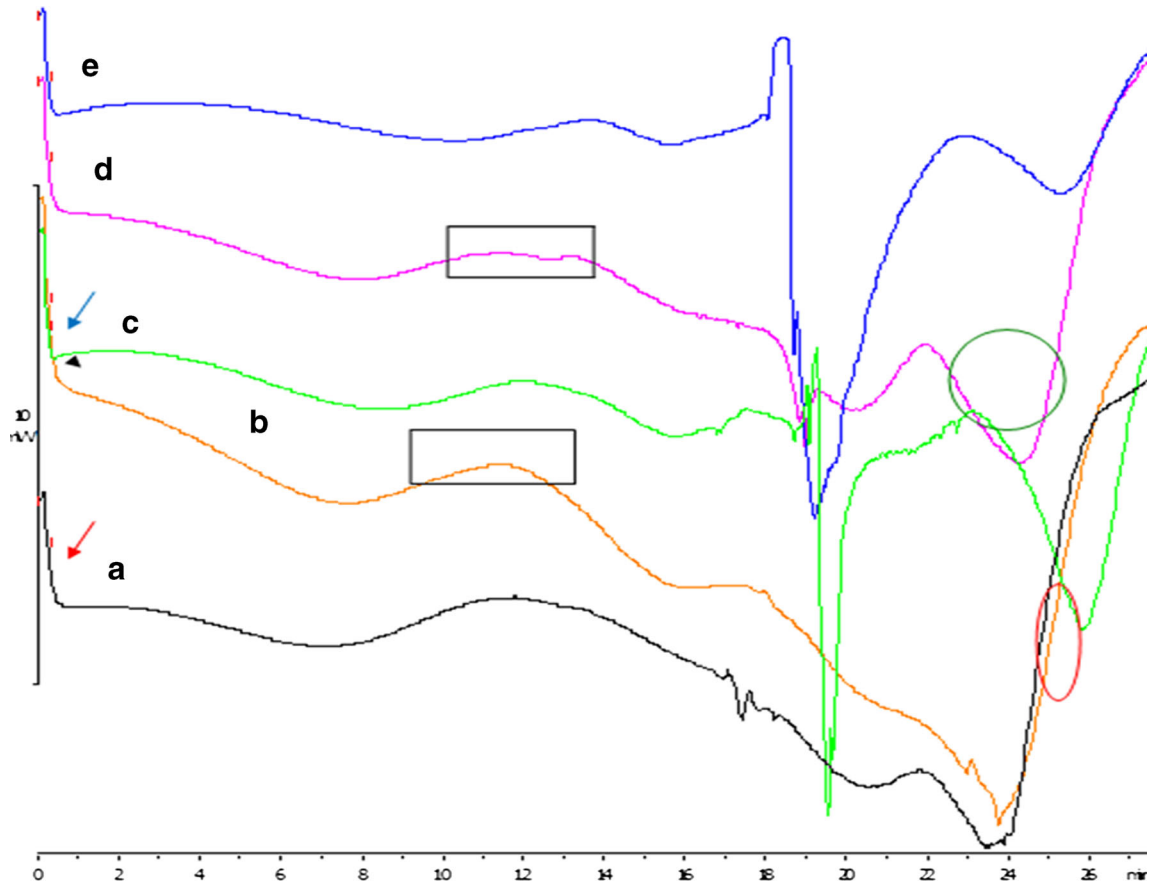

Fig. 2. Differential scanning calorimetry of semi-IPN films: **a** film 1, **b** film 9, **c** film 2, **d** film 10, and **e** film 6

easily on thermal exposure. Sarasam and Madihally (2005) (44) suggest that chitosan, a natural polymer, degrades at a temperature of 270°C prior to melting. Thus, it can be deduced that a temperature of 350°C will greatly impact the stability of natural polymers as the temperature range from 230 to 300°C already causes decomposition of polymeric material.

Structural Morphological Analysis of the Semi-IPN Films

Figure 3a–g demonstrates the SEM images of the semi-IPN films and the difference in surface morphologies of the films prepared using various polymer and crosslinker concentrations. Zhao *et al.* and Bhuvaneshwari *et al.* (45,46) have reported that the surface morphology of pure CS films is relatively smooth, nonporous, flat, and homogenous. However, with the introduction of a polymer IPN, the addition of bioactives and crosslinking modification to the surface revealed a slightly rough surface texture with the existence of pores and cracks in some instances, confirming a porous network microstructure which is one of the essential features required to optimize gaseous exchange at the wound site. Porous structures were clearly observed in all micrographs of films but the pore size and shape differed as shown in Fig. 3e (film 6) which had a slightly more rough surface topology with pores that were elongated and small in shape, whereas film 10 (Fig. 3g) showed a surface morphology with a more fibrous-like structure, pores tend to be long, larger, and rod-like in shape. Film 9 (Fig. 3f) showed pores that are much larger and clearly hollow with a definite border, whereas film 1 (Fig. 3c) and film 2 (Fig. 3d) showed a similar surface morphology with randomly orientated pores that are indefinite in size, shape, and structure with the presence of a few cracks on the film surface. These differential surface features were attributed to the different polymer concentration and degree of crosslinking in the respective films. Film 9 (Fig. 3f) and Film 10 (Fig. 3g) have the highest quantity of crosslinker relating to the greatest degree of crosslinking therefore these films

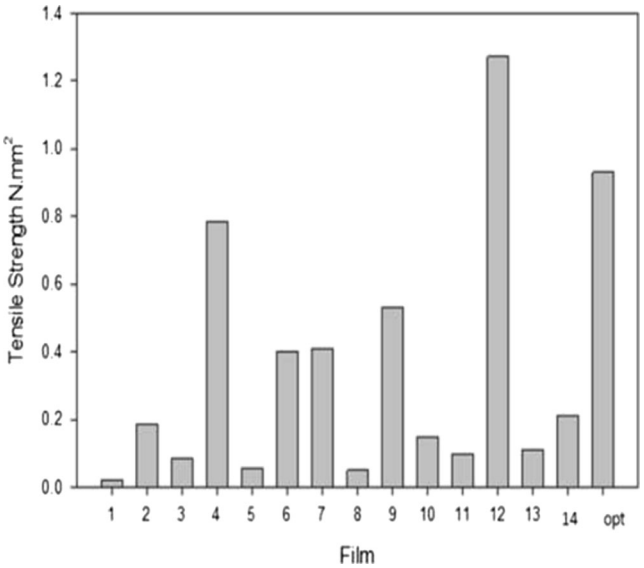

Fig. 4. Tensile strength (N mm^2) of the various semi-IPN Films

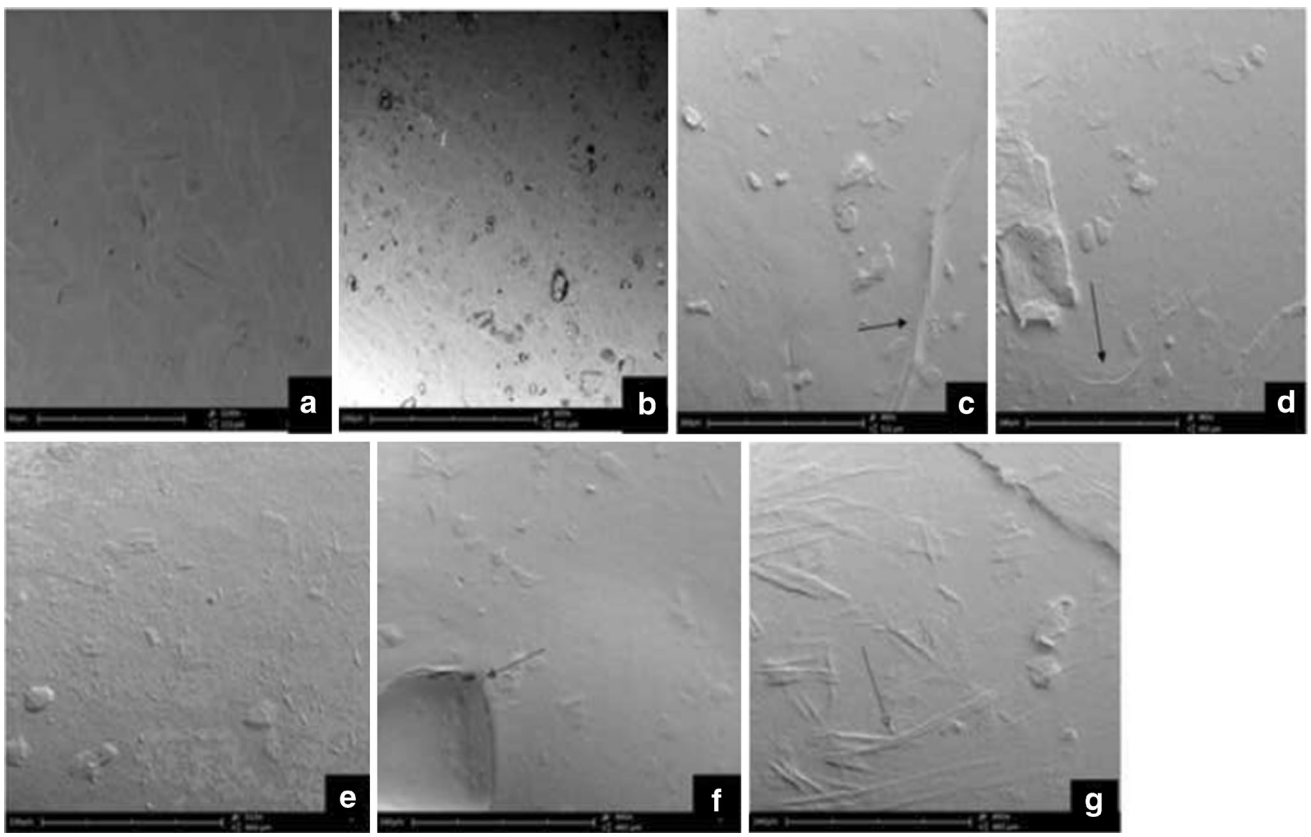

Fig. 3. Scanning electron micrographs of semi-IPN films: **a**, **b** optimized film, **c** film 1, **d** film 2, **e** film 5, **f** film 9, and **g** film 10

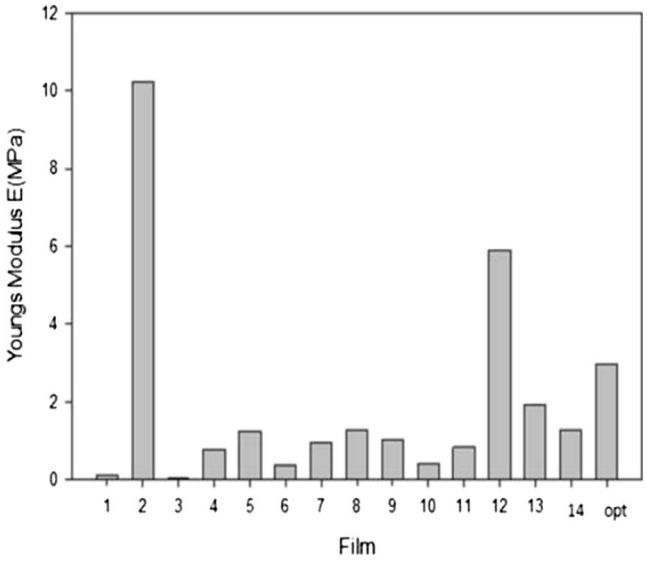

Fig. 5. Young modulus E (MPa) for various film formulations *via* nano-Tensile analysis

exhibit larger pores. However, distinguishing features of pores of the various films such as those in film 9 (Fig. 3g) and film 10 (Fig. 3f) could be accounted to a lower concentration of CS at 3% and higher CS concentrations of 1% being used in film 9 (Fig. 3g) and film 10 (Fig. 3f), respectively. A lower degree of crosslinking results in cracks within the surface due to poor tensile properties as observed for film 2 (Fig. 3d). When both the crosslinker and CS were used in intermediate quantities in films, the pores were notably smaller and the surface topology was rougher relating to the percentage crystallinity as observed in film 5 (Fig. 3e).

Textural Profile Analysis and Young's Modulus Determination of the Semi-IPN Films

The tensile and mechanical properties of all films were investigated by textural and nanotensile analysis. Figures 4 and 5 show that an increase in polymer concentration yielded a greater Young's modulus (YM) and tensile strength values as presented by film 12. A greater degree of rigidity and stiffness is observed in film 12 as an increase in crosslinking and polymeric concentration affects the polymer backbone formation and polymer chain flexibility which inevitably have an impact on the stress–strain relationship of the film. Semi-IPN films with a smaller YM value showed defined flexibility and thus a limited amount of stress was required to produce a relatively high amount of strain. Figure 6 illustrates the linear portion of the slope showing linear elastic deformation at this point thus an optimized, fairly flexible film will have a relatively small YM value as it is representative of both the rigidity and stiffness of the films. Interestingly, when an intermediate quantity of crosslinker was used (0.25% *w*/*v*), the ultimate strength (σu) was the greatest among all films as can be seen in films 4, 5, 7, 12, and 14, represented by the highest point on the stress–stain curve (Fig. 6). However, films with a high σu value were also likely to have a high YM value as ultimate strength and YM are directly proportional and thus have poorer flexibility and elastic properties. Thus, the degree of crosslinking and polymer concentration has a distinct effect on elasticity and flexibility of films as ultimately a

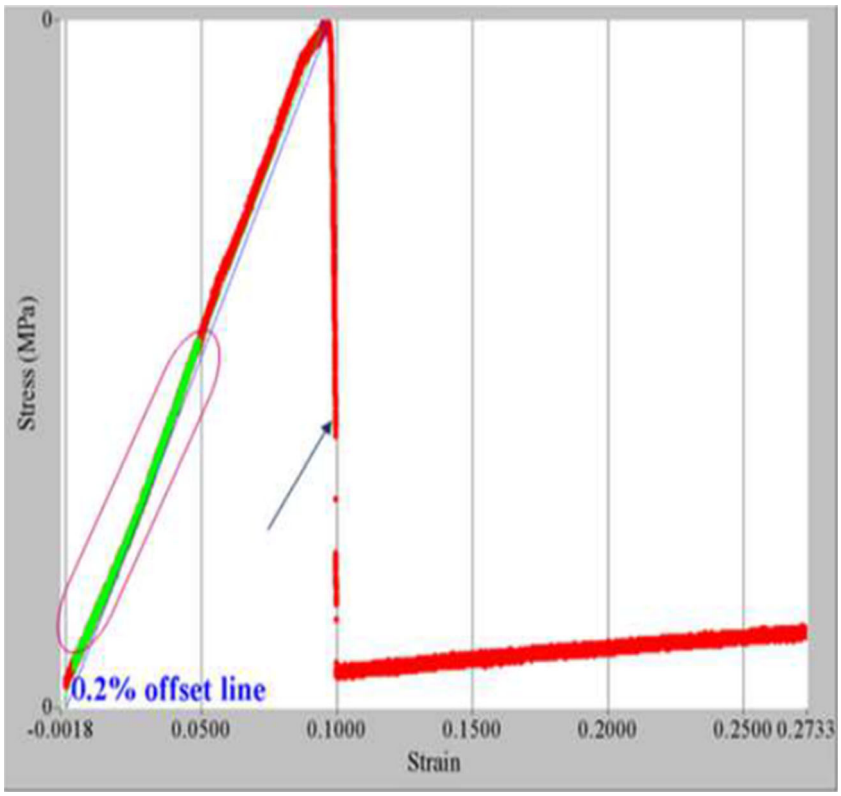

Fig. 6. Stress–strain nano-Tensile profile and Young's modulus

higher percentage causes a distinct increase in film rigidity and stiffness. Giovino *et al.* and Boatang *et al.* (47,48) reported on the use of glycerol in films as a plasticizer to improve film properties and prevent damage, therefore the addition of glycerol also greatly improves the flexibility and elasticity index of films. Improved flexibility properties were imparted by the formation of H-bonding of glycerol with CS and at the same time ensuring the semidestruction of hydrogen network formation by the breakage of both intramolecular and intermolecular bonds.

Swelling Capacity and Equilibrium Water Content Analysis of the Semi-IPN Films

The swelling capacity, water absorption, and equilibrium water content are important factors when considering the rate of absorption of polymeric films when in contact with the skin surface. Thus, the swelling capacity (%) and equilibrium water content (%) was evaluated in phosphate buffer solution (37°C; pH 7.4) (Figs. 7 and 8). Both plots clearly revealed that film 11, film 13, followed by film 2 had the greatest swelling capability occurring within the first hour after immersion (Fig. 8). This can be directly attributed to the low crosslinker concentration, thus covalent bond formation between polymers and polymer chains occur to a lesser extent providing enhanced hydrodynamic free volume to accommodate more water molecules, therefore exhibiting a greater swelling capacity. Poor crosslinking resulted in an increase in porosity which leads to fast initial rates of liquid uptake and a higher extent of equilibrium swelling. This suggests that a faster onset, degree and rate of bioactive absorption will occur. When the concentration of crosslinker was increased as in films 6, 8, 9, 2, and 14, the swelling capacity and water content decreased due to greater covalent bond formation overcoming porous sites, thus allowing penetration and absorption to occur at a reduced rate. This ensures sustained release of the bioactive (curcumin) throughout every stage of the wound healing phase (*i.e.* inflammation, granulation, proliferation, and remodeling). Thus, it can be deduced that the overall delivery rate of bioactive material (curcumin) was dependent on the rate of swelling as a decrease in the swelling rate promoted long lasting and controlled release of bioactive.

Water Vapor Transmission Rate Analysis

Figure 9 represents the effects of various polymer concentrations on the water vapor transmission rate (WVTR). In the case of wounds, particularly burn wounds, the WVTR plays a key role with regard to moisture balance as it needs to be maintained throughout the repairing process. A low WVTR value could lead to numerous clinical challenges due to the buildup of exudates, whereas a very high value can lead to wound dehydration that decelerates the healing process. Furthermore, Sung *et al.* and Queen (49,50) stated that a transmission rate between 2,000 and 2,500 g/m^2 per day would yield the adequate moisture environment for optimal healing. In this study, it was deduced that the highest WVTR value was seen in film 12 where a high concentration of polymer and crosslinker was used, thus promoting wound dehydration. Furthermore, it was noted that the WVTR value increased with an increased quantity of CS rather than hypromellose. Thus, it can be deduced that the WVTR value

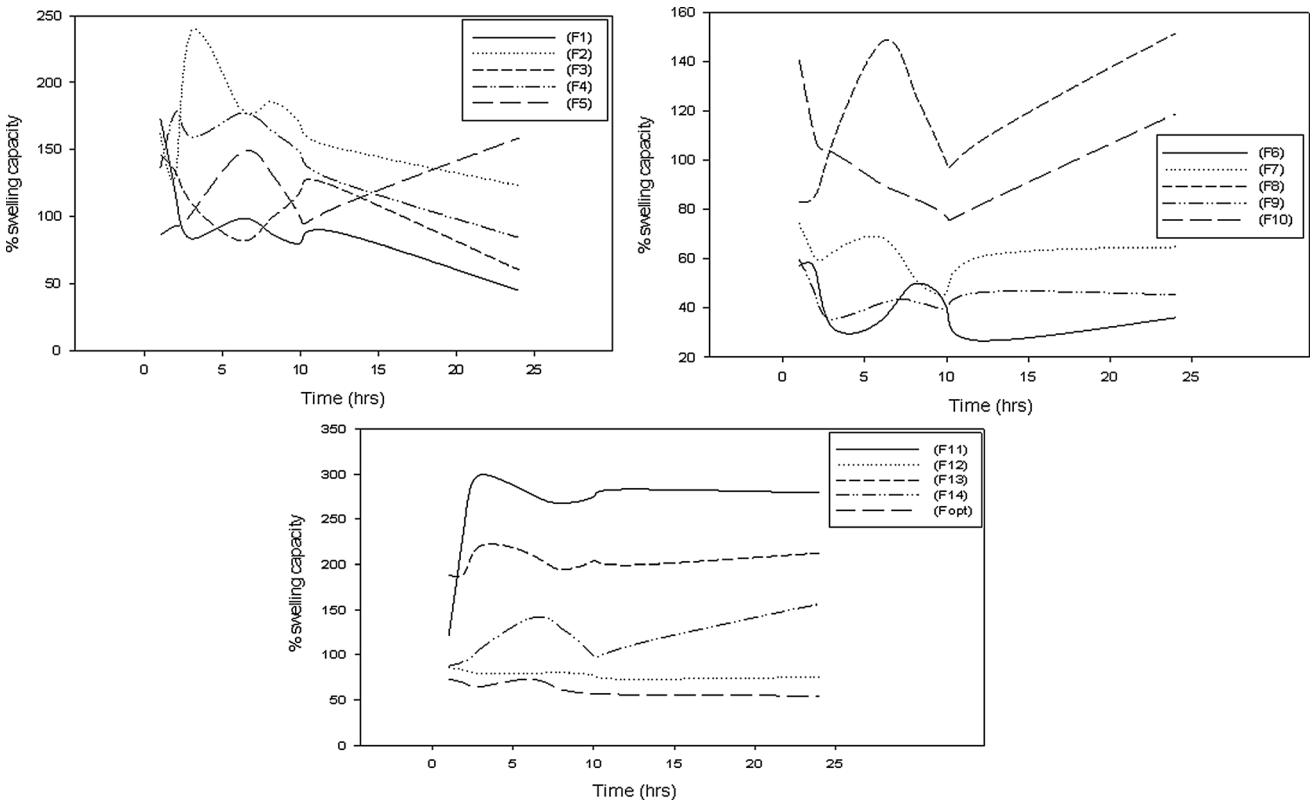

Fig. 7. Profile of swelling capacity of the semi-IPN films 1–14 and the optimized film

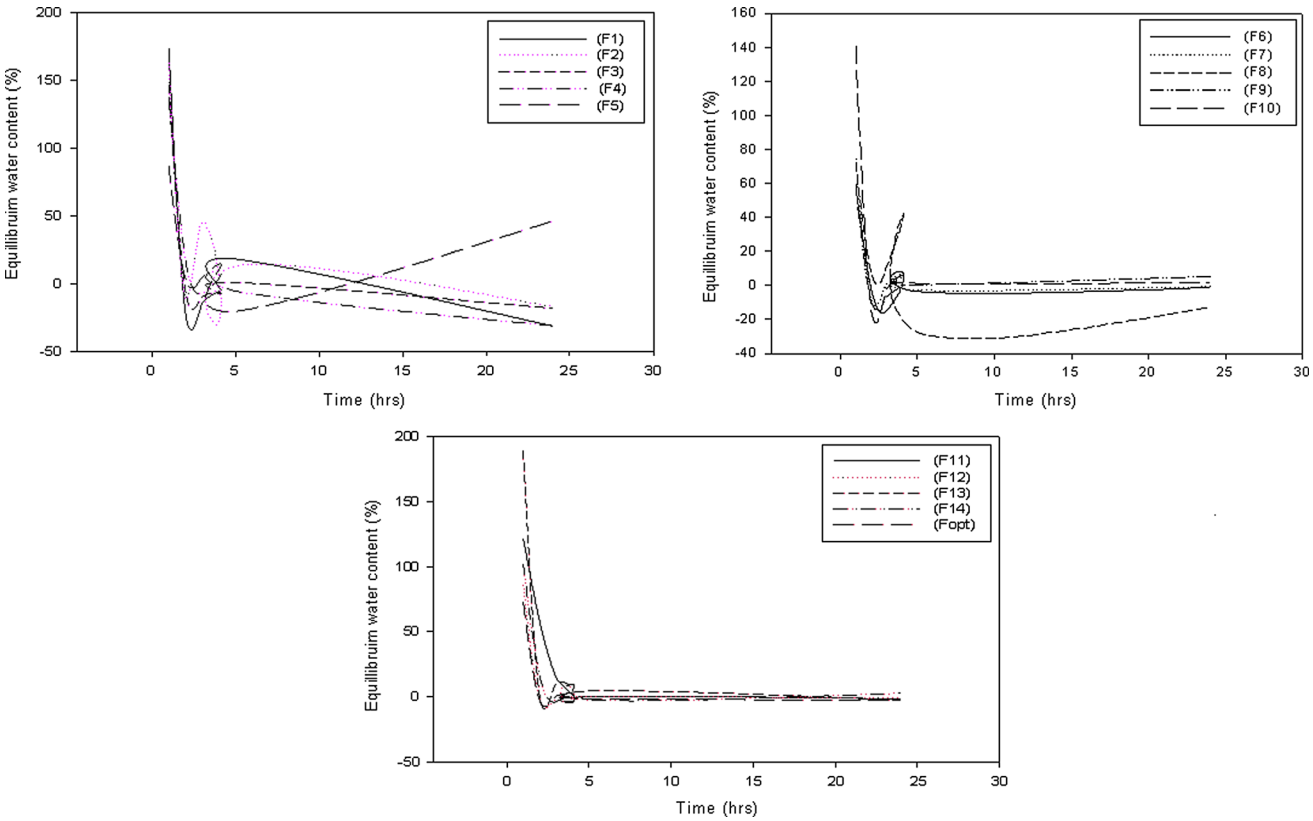

Fig. 8. Profile of equilibrium water content of the semi-IPN films 1–14 and the optimized film

was directly proportional to the CS concentration and therefore for optimal gaseous exchange, an intermediate quantity of polymer and crosslinker was required as observed in film 5a and b.

Rheological Characterization of the Semi-IPN Film Polymer Blends

Table V represents the rheological characteristics in particular viscosity and yield stress of formulation blends. From the results obtained, films 3, 11, and 13 have the lowest shear viscosity rates and this can be attributed to low-percentage crosslinking, suggesting weaker bonds due to lower chemical interactions between the amine groups of CS and genipin. Interestingly, it was noted that the degree of shear rate was directly proportional to the concentration of CS and the quantity of crosslinker used. At higher concentrations of CS (as in film 2) where 3% CS was used, hydrodynamic volume expansion occurred, which resulted from the protonated NH_3 groups caused by repulsive forces thus increasing the shear rate (51). Furthermore, when higher concentrations of crosslinker was used such as 0.025% (films 1, 4, 5, 7, 8, and 14), the viscosity shear rate increased. Stronger interactions due to a greater extent of crosslinking resulted in a remarkable increase in shear viscosity. The yield stress under experimental conditions can be defined as that stress under which no flow can be observed and is related to the polymer viscosity (52). From Table V, it is observed that lower viscosity rates such as those in films 9–11 resulted in a weaker yield. Thus, semi-IPN films are able to exhibit greater strain results when a stress is applied in the presence of a high yield stress. This directly influences the elasticity of the films which is an important property regarding wound dressings for topical use. From the results obtained, it can be noted that the best rheological and mechanical properties will be observed in films 2, 4, 12, 14, and the optimized film. Post characterization of semi-IPN films generated through the Box-Behnken experimental design lead to an ultimate optimal formulation of 3% CS, 0.1% genipin, and 0.4% hypromellose. This optimized formulation was further subjected to *in vitro* and *ex vivo* studies.

Bioevaluation of the Curcumin-loaded Semi-IPN Film

A transdermal permeation and release study was undertaken on the optimum candidate formulation obtained. Bioactive release and permeation studies of curcumin are depicted in Fig. 10a, b. Interestingly, an initial burst release is observed within both systems at 1.1 mg (bioactive release) and 2.23 mg (bioactive permeation) within the first hour but is more pronounced during the permeation study. The first phase of the healing process is inflammation and begins within a few minutes of injury and may last up to 24 h or longer (53), thus an initial burst release as seen initiates the delivery of curcumin at the wound site thus potentiating a therapeutic anti-inflammatory and antibacterial therapeutic effect at the wound site in association to inflammation. Furthermore, throughout this study, it can be noted that bioactive release occurs at a greater rate when permeated through the skin when released alone. This can be directly attributed to the hydrophobic nature of curcumin, thus enhanced release rates

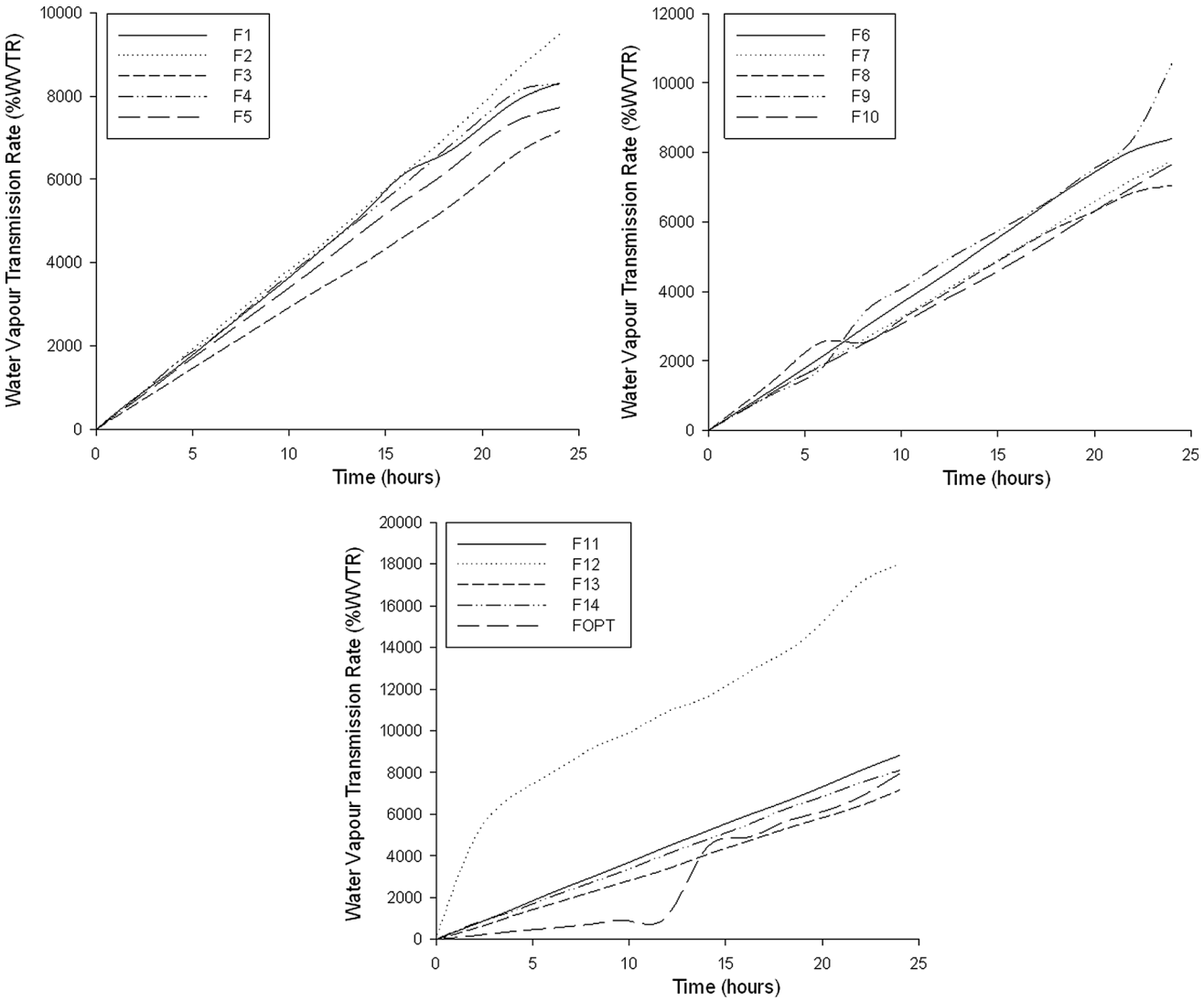

Fig. 9. Profile of the rate of water vapor transmission within the semi-IPN films 1–14

Table V. Effects of Various Concentrations of Polymer and Crosslinker on the Formulation Viscosity and Yield Stress for Film Formation

Formulation no.	Viscosity at a shear rate of 100 s^{-1} (MPa)	Yield stress (Pa)
F1	742.51	20.97
F2	605.36	38.55
F3	32.93	38.46
F4	529.48	38.59
F5	578.53	38.52
F6	219.67	38.63
F7	516.38	38.62
F8	579.62	38.62
F9	115.27	29.65
F10	40.92	32.29
F11	6.51	25.03
F12	46.85	38.51
F13	1.24	9.97
F14	578.32	38.57
F optimized	62.53	38.59

will be observed when in contact with skin tissue as preferential interactions occur with lipid-based membranes such as the phospholipid bilayer present in the skin. Therefore, this directly impacts the major barrier associated with curcumin release improving its bioavailability and clinical efficacy (54). The stratum corneum of the skin only allows moderately lipophilic molecules that are small to partition across it passively, into the deeper layer of the skin (54). The stratum corneum is not an inert structural material and behaves as a reactive medium that may alter in response to changes in the sorption or desorption of penetrant molecules, thus deviation to Fick's law occurs (55) as can be seen in Fig. 10c. Between 4 and 6 h, an intermediate second burst release was seen in Fig. 10b from 3.39 to 6.19 mg, thus further potentiating a deviation from Fick's law. The flux rate of permeated bioactive release reveals substantial deviation, thus revealing that steady-state release profiles are not maintained throughout the study (Fig. 10c). Therefore, curcumin-loaded IPN films will serve as a dressing with ideal characteristics intended to be applied topically to wounds. Variation to steady-state release profiles potentiating wound healing

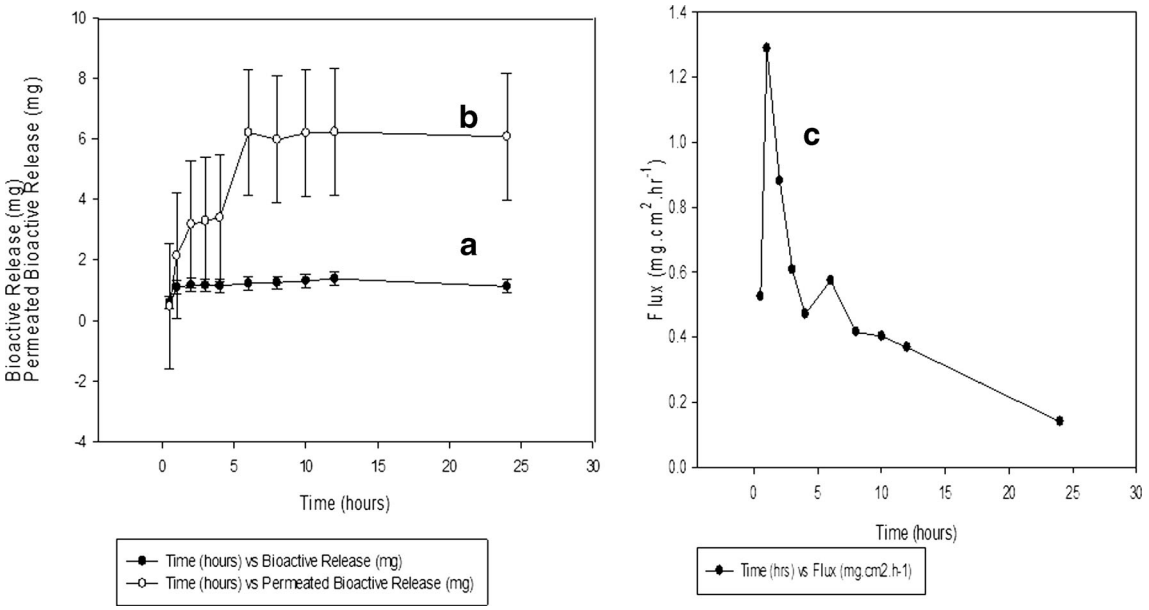

Fig. 10. **a** Drug release profile of curcumin-loaded semi-IPN films and **b** drug release permeation through the Sprague-Dawley rat, **c** *ex vivo* permeation profile of a curcumin-loaded semi-IPN film through excised skin tissue of Sprague-Dawley rats

is further supported by Seetharaman *et al.* (56) whom also state that ideal characteristics for wound healing is potentiated by this type of release. When considering factors that affect the permeation rate across skin tissue, evaluation of characterization studies such as the FTIR analysis discussed in text, it can be seen that introduction of crosslinking by genipin resulted in the formation of crosslinking bridges at the aromatic site thus supporting the formation of a crosslinked network. This brought about an increase in intermolecular conjugation. Augmentation of crosslinking resulted in greater mechanical properties such as an elevated Young's modulus which could be seen as the crosslinking increased thus forming stiffer and more rigid films. Therefore, an increase in crosslinking decreases the permeation ability as a denser network structure occurs. Rana *et al.* (57) also state that stronger crosslinking of chitosan by increasing the crosslinker concentration seems to restrict the permeation of drug.

CONCLUSIONS

The novel semi-IPN film composed of CS and its derivatives, crosslinked and incorporated with a bioactive (curcumin), was developed in view to create an advanced delivery system with the potential of wound healing due to therapeutic properties provided by polymers used. Medium molecular weight CS was dissolved in citric acid and successfully crosslinked with genipin before the incorporation of biopolymers such as hypromellose and curcumin in a stepwise manner to structure an IPN that ensured the bioactive can be gradually diffused through the Sprague-Dawley rat skin model. The films have shown the potential to swell and release the bioactive to stimulate proliferation, differentiation, and remodeling of the targeted skin tissue. This can be achieved as all biopolymers have active healing properties and thus the formation of a semi-IPN film will allow these properties to be synergistically combined to provide a therapeutic healing effect as discussed without the use of conventional drugs. Thus, it can be concluded that the semi-IPN film can positively influence the process of healing effectively with only the use of biomaterials providing biocompatible, bioadherent, nontoxic, and bioresorbable properties for effective wound healing.

ACKNOWLEDGEMENTS

This work was funded by the National Research Foundation (NRF) of South Africa.

Conflict of Interest The Authors declare that there are no conflicts of interest.

REFERENCES

1. Boatang JS, Matthews KH, Stevens HNE, Eccleston GM. Wound healing dressings and drug delivery systems. A review. J Pharm Sci. 2008;97(8):2892–900.
2. Abdelrahman T, Newton H. Wound dressings: principles and practice. Surgery (oxford). 2011;29:491–5.
3. Atiyeh BS, Hayek SN, Gunn SW. New technologies for burn wound closure and healing; review of the literature. Burns. 2005;31:944–56.
4. Singer AJ, Dagum AB. Current management of acute cutaneous wounds. N Engl J Med. 2008;359:1037–46.
5. Tanihara Y, Suzuki Y, Nishmura Y, Suzuki K, Kakimara Y. Thrombin sensitive peptide linkers for biological signal responsive drug release systems. Peptides. 1998;19:421–5.
6. Suzuki Y, Tanihara M, Nishmura Y, Suzuki K, Kakimara Y, Shimizu Y. A novel wound dressing with an antibiotic delivery system stimulated by microbial infection. ASA10 J. 1997;43:854–7.

7. Kim HJ, Choi EJ, Oh JS, Lee HC, Park SS, Cho CS. Possibility of wound dressing using poly(L-Leucin)/poly(ethylene glycol)/poly(L-Leucin) triblock copolymer. Biomaterials. 2000;21:131–41.
8. Hashimoto T, Suzuki Y, Tanihara M, Kakimara Y, Suzuki K. Development of alginate wound dressings linked with hybrid peptides derived from laminin and elastin. Biomaterials. 2004;25:1407–14.
9. Choi YS, Hong SR, Lee YM, Song KW, Park MH, Nam YS. Study on gelatine containing artificial skin. I Preparations and characteristics of novel gelatine-alginate sponge. Biomaterials. 1999;20:409–17.
10. Ma L, Gao C, MaO Z, Zhou J, Shen J, Hu X, *et al*. Collagen/chitosan porous scaffolds with improvised biostability for skin tissue engineering. Biomaterials. 2003;24:4833–41.
11. Li X, Chen J, Zhang B, Li M, Diao K, Zhong Z, *et al. In-situ* injectable nano-composite hydrogel composed of curcumin, N,O-Carboxymethyl chitosan and oxidised alginate for wound healing applications. Int J Pharm. 2012;437:110–9.
12. Muzarelli RA, Guerrieri M, Goteri G, Muzarelli C, Armeni T, Ghiselli R, *et al*. The biocompatibility of dibutyryl chitin in the context of wound dressings. Biomaterials. 2005;26:5844–54.
13. Kim BS, Gao H, Argum AA, Matyjaszewski K, Hammond P. All star polymer multilayers as pH responsive nanofilms. Macromolecules. 2009;42:368–75.
14. Crowder ML, Gooding CH. Spiral wound, hollow fibre membrane modules: a new approach to higher mass transfer efficiency. J Membrane Sci. 1997;137:17–29.
15. Hwang JJ, Stupp SI. Poly(amino acid) bioadhesives for tissue repair. J Biomater Sci Polymer. 2000;11:1023–38.
16. Dash M, Chiellini F, Ottenbrite RM, Chiellini E. Chitosan—A versatile semi-synthetic polymer in biomedical applications. Prog Polym Sci. 2011;36:981–1014.
17. Datta HS, Mitra SK, Partwarden B. Wound healing activity of topical application forms based on Ayurvedav. Evid Based Complement Alternat Med. 2011;2011:134378.
18. Ponnusamy S, Zinjarde S, Bhargava S, Rajamohanan PR, Ravikumar A. Discovering bisdemethoxycurcumin from *Curcuma longa* rhizome as a potent small molecule inhibitor of human pancreatic a-amylase, a target for type-2 diabetes. Food Chem. 2012;135:2638–42.
19. Kurup VP, Barrios CS. Immunomodulatory effects of curcumin in allergy. Mole NutrI and Food Res. 2008;52:1031–9.
20. Adaramoye OA, Anjos RM, Almeida MM, Veras RC, Silvia DF, Oliviera FA, *et al*. Hypotensive and endothelium-independent vasorelaxant effects of methanolic extract from *Curcuma long*a L in rats. J Ethnopharmacol. 2009;124:457–62.
21. Dao TT, Nguyen PH, Wonb HK, Kim EH, Park J, Wond BY, *et al*. Curcuminoids from *Curcuma longa* and their inhibitory activities on influenza A Neuraminidases. Food Chem. 2012;134(1):21–8.
22. Sidhu GS, Singh AK, Thaloor D, Banaudha KK, Pathaik GK, Srimal RC, *et al*. Enhancement of wound healing by curcumin in animals. Wound Repair Regen. 1998;6(2):167–77.
23. Mani H, Sidhu GS, Kumari R, Gaddipati JP, Seth P, Maheshwari RK. Curcumin differentially regulates TGF-β1, its receptors and nitric oxide synthase during impaired wound healing. Biofactors. 2002;16:29–43.
24. Topham J. Why do some cavity wounds treated with honey or sugar paste heal without scarring. J Wound Care. 2002;11(2):53–5.
25. Beppu MM, Vieira RS, Aimoli CG, Santana CC. J Membr Sci. 2007;301:126.
26. Pauliukaite R, Ghica ME, Fatibello-Filho O, Brett CMA. Anal Chem. 2009;81:5364.
27. Singh A, Narvi S, Dutta P, Pandey N. Bull Mater Sci. 2006;29:233.
28. Machado MO, Lopes ECN, Sousa KS, Airoldi C. Carbohydr Polym. 2009;77:760.
29. Pujana MA, Perez-Alverez L, Iturbe LCC, Katime I. Biodegradible chitosan nanogels crosslinked with genipin. Carbohydr Polym. 2013;94(2):836–42.
30. Gao L, Gan H, Meng Z, Gu R, Wu Z, Zhang L, *et al*. Effects of genipin cross-linking of chitosan hydrogels on cellular adhesion and viability. Colloids Surf B: Biointerfaces. 2014;117:398–405.
31. Yan LP, Wang YJ, Ren L, Wu G, Caridade SG, Fan JB, *et al*. Genipin crosslinked collagen/chitosan biomimetic scaffolds for articular cartilage tissue engineering applications. J Biomed Mater Res Part A. 2010;95A:2.
32. Huang LLH, Sung HW, Tsai CC, Huang DM. Biocompatibility studies of a biological tissue fixed with a naturally occurring crosslinking reagent. J Biomed Mater Res. 1998;42:568–76.
33. Mi FL, Tan YC, Liang HF, Sung HW. In vivo biocompatibility and degradability of a novel injectable-chitosan-based-implant. Biomaterials. 2002;23:181–91.
34. Wu W, Liu J, Cao S, Tan H, Li J, Xu F, *et al*. Drug release behaviour of a pH sensitive semi-interpenetrating polymer network hydrogel composed of poly (vinylalcohol) and star poly (2-dimethyl amino) ethyl mecrylate. Int J Pharm. 2011;416(1):104–9.
35. Zhang JT, Huang SW, Zhuo RX. Temperature sensitive polyamidoamine dendrimer/poly (N-isopropyl/acrylamide) hydrogels with improved responsive properties. Macromolecules, Biosc. 2004;4:575–8.
36. Yao F, Xu LQ, Fu GD, Lin BP. Sliding graft interpenetrating polymer network from simultaneous "click chemistry" and atom transfer radical polymerisation. Macromolecules. 2010;43:9761–70.
37. Liu YY, Fan XD, Wei BR, Si QF, Chen WX, Sun L. Ph responsive amphillic hydrogel networks with IPN structure: a strategy for controlled drug release. Int J Pharm. 2006;308:205–9.
38. Saimani S, Dal-Cin MM, Kumar A, Kingston DM. Separation performance of asymmetric membranes based on PEGDa/PEI semi-interpenetrating polymer network in pure and binary gas mixtures of CO_2, N_2 and CH_2. J Membr Sci. 2010;362:353–9.
39. Bindu TVL, Vidyavathi M, Kavitha K, Sastry TP, Suresh Kumar RV. Preparation and evaluation of chitosan-gelatin composite films for wound healing activity. Trends Biomater Artif Organs. 2010;24(3):123–30.
40. Kim IY, Yoo MK, Seo JH, Park SS, Na H, Lee HC, *et al*. Evaluation of semi-interpenetrating polymer networks composed of chitosan and polyxamer for wound dressing applications. Int J Pharm. 2007;341:35–43.
41. Shaikh RP, Kumar P, Choonara YE, du Toit LC, Pillay V. Crosslinked electrospun nanofibrous membranes: elucidation of their physicochemical, physicomechanical and molecular disposition. Biofabrication. 2012;4:025002. 21 pp.
42. Amnuaikit C, Ikeuchi I, Ogawara K-I, Higaki K, Kimura T. Skin permeation of propranolol from polymeric film containing terpene enhancers for transdermal use. Int J Pharm. 2005;289:167–78.
43. Davies DJ, Ward RJ, Heylings JR. Multi-species assessment of electrical resistance as a skin integrity marker for in vitro percutaneous absorption studies. Toxicol in Vitro. 2003;18:351–8.
44. Sarasam A, Madihally SV. Characterisation of chitosan-polycaprolactone blends for tissue engineering applications. Biomaterials. 2005;26(27):5500–8.
45. Zhao QS, Ji QX, Xing K, Li XY, Liu CS, Chen XG. Preparation and characteristics of novel porous hydrogel films based on chitosan and glycerophosphate. Carbohydr Polym. 2009;76:410–6.
46. Bhuvaneshwari S, Sruthi D, Sivasubramanian V, Niranjana K, Sugunabai J. Development and characterization of chitosan films. Int J Eng Res and Appl (IJERA). 2000;1(2):292–9.
47. Giovino C, Ayensu I, Tetteh J, Boateng JS. Development and characterisation of chitosan films impregnated with insulin loaded PEG-b-PLA nanoparticles (NPs): a potential approach for buccal delivery of macromolecules. Int J Pharm. 2012;428:143–51.
48. Boatang JS, Pawar HV, Tetteh J. Polyox and carrageenan based composite film dressing containing anti-microbial and anti-inflammatory drugs for effective wound healing. Int J Pharm. 2013;441(1–2):181–91.
49. Sung JH, Hwang MR, Kim JO, Lee JH, Kim YI, Kim JH, *et al*. Gel characterisation and in vivo evaluation of minocycline-loaded wound dressing with enhanced wound healing using polyvinyl alcohol and chitosan. Int J Pharm. 2010;392:232–40.
50. Queen D, Gaylor JDS, Evans JH, Courtney JM, Reid WH. The preclinical evaluation of the water vapour transmission rate through burn wound dressings. Biomaterials. 1987;8:367–71.

51. Pakravan MP, Heuzey MC, Ajji A. A fundamental study of Chitosan/PEO electrospinning. Polymer. 2011;52:4813–24.
52. Barnes HA, Walter K. The yield stress myth? Rheol Acta. 1985;24:323–6.
53. Pawar HV, Tetteh J, Boateng JS. Preparation, optimisation and characterisation of novel wound healing film dressings loaded with streptomycin and diclofenac. Colloids Surf B: Biointerfaces. 2013;102:102–10.
54. Zhao YS, Lu CT, Zhang Y, Xiao J, Zhao YP, Tian JL, *et al*. Selection of high efficient transdermal lipid vesicle for curcumin skin delivery. Int J Pharm. 2013;454:302–9.
55. Scheuplein RJ. Permeability of the skin. Handbook of physiology, Reactions to environmental agents. 2011; doi: 10.1002/cphy.cp090119.
56. Seetharaman S, Natesan S, Stowers RS, Mullens C, Baer DG, Suggs LG, *et al*. A PEGylated fibrin-based wound dressing with antimicrobial and angiogenic activity. Acta Biomater. 2011;7:2787–96.
57. Rana V, Babita K, Goyal D, Tiwary AK. Soduim citrate crosslinked chitosan films: optimisation and substitute for human/rat/rabbit epidermal sheets. J Pharm Pharmaceut Sci. 2005;8(1):10–7.